iScience

CellPress
OPEN ACCESS

Article

Acetylation halts missense mutant p53 aggregation and rescues tumor suppression in non-small cell lung cancers

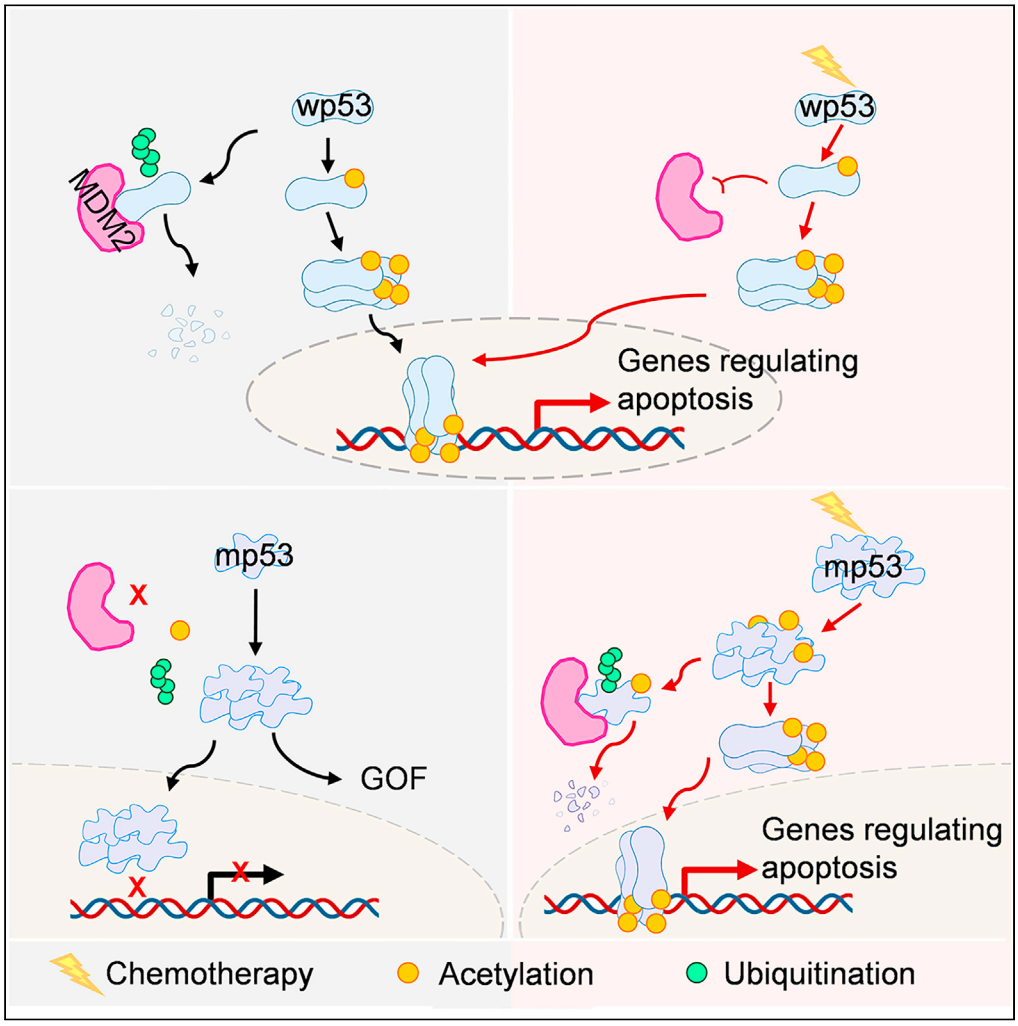

Daxing Xu, Wei Qian, Zhenkun Yang, ..., Zhening Pu, Peihua Lu, Jian Zou

puzhening@njmu.edu.cn (Z.P.)
lphty1_1@163.com (P.L.)
zoujan@njmu.edu.cn (J.Z.)

Highlights

Missense mutant p53 is correlated with chromosomal instability in NSCLC

Acetylation enhances mutant p53 ubiquitination and proteasome degradation

Acetylation halts aggregation and rescues tumor suppression of mutant p53 in NSCLC

Acetylated p53, but not p53, is a promising prognosis for patient with NSCLC

Xu et al., iScience *26*, 107003
July 21, 2023
https://doi.org/10.1016/j.isci.2023.107003

iScience

CellPress
OPEN ACCESS

Article

Acetylation halts missense mutant p53 aggregation and rescues tumor suppression in non-small cell lung cancers

Daxing Xu,[1,2,6] Wei Qian,[1,2,6] Zhenkun Yang,[1,2,6] Zhenhao Zhang,[1,2,6] Ping Sun,[3,6] Quan Wan,[4] Ying Yin,[1,2] Yaling Hu,[1,2] Lingli Gong,[1,2] Bo Zhang,[1,2] Xusheng Yang,[1,2] Zhening Pu,[1,2,*] Peihua Lu,[2,5,*] and Jian Zou[1,2,7,*]

SUMMARY

***TP53* mutations are ubiquitous with tumorigenesis in non-small cell lung cancers (NSCLC). By analyzing the TCGA database, we reported that *TP53* missense mutations are correlated with chromosomal instability and tumor mutation burden in NSCLC. The inability of wild-type nor mutant p53 expression can't predict survival in lung cancer cohorts, however, an examination of primary NSCLC tissues found that acetylated p53 did yield an association with improved survival outcomes. Molecularly, we demonstrated that acetylation drove the ubiquitination and degradation of mutant p53 but enhanced stability of wild-type p53. Moreover, acetylation of a missense p53 mutation prevented the gain of oncogenic function observed in typical *TP53* mutant-expressing cells and enhanced tumor suppressor functions. Consequently, acetylation inducer targeting of missense mutant p53 may be a viable therapeutic goal for NSCLC treatment and may improve the accuracy of current efforts to utilize p53 mutations in a prognostic manner.**

INTRODUCTION

TP53 coding p53 protein is a transcriptional regulator responsible for guarding genome stability and regulating crucial cellular processes from differentiation and proliferation to metabolism and senescence/death.[1] *TP53* is the gene most highly correlated with tumorigenesis in humans, with approximately 50% of cancers containing the *TP53*/p53 variation according to data from The Cancer Genome Atlas (TCGA).[2] p53 mutations or alterations are associated with chromosomal instability, such as oncogene amplification and tumor suppressor gene deletion. Mutated p53 tumors predominantly exhibit abnormal expression of cell cycle progression genes and apoptosis related genes/proteins, which are significantly associated with the decreased survival rate of patients with multiple cancers.[3–6]

Lung cancer involves malignant tumors with some of the highest morbidity and mortality rates, of which non-small cell lung cancer (NSCLC) accounts for 75% of all cases and causes about 85% of lung cancer-related deaths.[7,8] *TP53* mutation is one of the most common mutations in NSCLC.[9–11] In stage I NSCLCs, the survival of wild-type *TP53* patients is higher than that of a patient with mutant *TP53*. Despite the *TP53* mutation having no significant correlation with patient survival, it has been shown to be significantly correlated with recurrence in advanced NSCLCs.[12–14] An integrated analysis of *TP53* and pathway alterations indicated that *TP53* mutation fails to predict overall survival of lung adenocarcinoma (LUAD) patients. However, among patients with *TP53* mutation, those with high levels of CDC20, PLK1, CENPA, and KIF2C had a relatively poorer survival. Therefore, it is not recommended to assess prognosis based solely on *TP53* gene status.[2]

The majority of p53 mutations are missense mutations caused by a single amino acid substitution. p53 missense mutations mainly occur within the DNA-binding domain (DBD), resulting in loss of DNA-binding ability.[15] Although it is widely held that p53 missense mutations largely contribute to the malignant phenotype of tumor cells, meta-analysis indicates that p53 missense mutations do not predict poor survival outcomes.[2] Thus, whether missense mutations endow **gain-of-function (GOF)** or trigger loss of guardian functions remains controversial.[16,17]

[1]Department of Laboratory Medicine, The Affiliated Wuxi People's Hospital of Nanjing Medical University, Wuxi, Jiangsu 214023, China

[2]Center of Clinical Research, The Affiliated Wuxi People's Hospital of Nanjing Medical University, Wuxi, Jiangsu 214023, China

[3]Department of Pathology, Jiangnan University Medical Center, Wuxi, Jiangsu 214023, China

[4]Department of Neurosurgery, Jiangnan University Medical Center, Wuxi, Jiangsu 214023, China

[5]Department of Medical Oncology, The Affiliated Wuxi People's Hospital of Nanjing Medical University, Wuxi, Jiangsu 214023, China

[6]These authors contributed equally

[7]Lead contact

*Correspondence: puzhening@njmu.edu.cn (Z.P.), lphty1_1@163.com (P.L.), zoujan@njmu.edu.cn (J.Z.)

https://doi.org/10.1016/j.isci.2023.107003

Attributed to ubiquitin-mediated degradation, normal p53 is a short-lived transcriptional factor with a half-life of ~5–20 min, while p53 missense mutations contribute a longer half-life via escape from ubiquitin-mediated degradation.[18,19] These studies indicate that different mechanisms are involved in regulating wild-type and mutant p53 stability and biological functions. It is well-known that acetylation is required for the activation of p53 and subsequent biological processes, including contributing to wide-type p53 stability by inhibiting ubiquitination.[20,21] Six acetyltransferases have been identified to-date, which modify p53 at the lysine site of the C-terminal domain (CTD) or its central DBD. Six of the eight major acetylation sites of human p53 (K120, 164, 370, 372, 373, 381, 382, and 386) are in the CTD region.[22–24] p53 acetylation at these lysine (K) residues trigger a switch to glutamine (Q), inhibiting ubiquitination, subsequent degradation by MDM2, and release from transcriptional repressor binding (23, 25). Interestingly, p53 missense mutations rarely occur at lysine sites, especially in the CTD region.[25] Moreover, acetylation recovers the physical conformation and can restore missense p53 mutations, DNA binding, and tumor suppression.[26,27]

The present study applied high-throughput analysis to a large cohort of NSCLCs tissues spanning 17 previous studies via TCGA and in-house tissue arrays to explore the relationship between *TP53*/p53 gene status/expression and NSCLCs prognosis more in depth. Combined with functional experiments using an acetylation mimic mutant in CTD, it was revealed that higher p53 acetylation was positively correlated with survival outcomes. Additionally, acetylation halted the aggregation of missense mutated p53, reverses the GOF and rescues tumor suppression of missense mutated p53. This may be mechanically mediated through the regulation of ubiquitination and degradation, offering a theoretical basis for further study of the reversal of GOF p53 missense mutation acetylation.

RESULTS

TP53 missense mutation is correlated with chromosomal instability and tumor mutation burden in non-small cell lung cancers

We leveraged 17 previous studies on NSCLCs using TCGA online tools such as cBioPortal for analysis. Using 3238 of 6122 samples, we found that the overall *TP53* mutation frequency was 53%. The mutations for *TP53* included missense mutations at 64.88% (2219/3420), truncated mutations at 24.74% (846/3420), in-frame mutations at 1.46% (50/3420), splice mutations at 8.86% (303/3420), and gene fusions at 0.06% (2/3420) (Figure 1A). Among these mutations, the majority of missense mutations were observed in the DBD of *TP53*. "Hot spot" missense mutations included R273, R158, R248, G245, V157, G249, and R175 in order of mutation frequency (Figure 1B). Further analysis of nucleotide alteration of hot spot missense mutations showed that most of R158, V157, G245, R273, and G249 mutations were C > A substitutions, while more than 70% of R175 mutations were C > T substitutions (Figure 1C, left). The main amino acid substitution of these missense mutations was R273L, R158L, V157F, R249M, and R175H (Figure 1C, right). To determine the relationship between *TP53* missense mutations and genomic stability, the frequency of copy number variation (CNV), and somatic mutation (SMT) was analyzed from samples collected over 17 previous NSCLC studies using cBioportal for cancer genomics. A total of 1305 *TP53* missense mutated samples of 1114 patients and 2801 wild-type samples of 2651 patients were included. The frequency of CNV and SMT in the *TP53* missense mutation group was much higher than that in wild type group, and the number of genes with CNV and SMTs were also greater than in wild type group (Figures 1D and 1E). The data in Figures 1F and 1G represent the top 20 genes with CNV and SMT alterations between missense and wild type groups, respectively. Tumor mutation burden (TMB) analysis further indicated that the population containing missense mutated *TP53* observed higher gene mutations (Figure 1H). Therefore, these data suggest that *TP53* genetic alterations, missense mutations correspond to higher rates of chromosome instability events in NSCLC.

TP53 missense mutations are not necessarily associated with adverse outcomes in NSCLCs

Utilizing NSCLC TCGA sample data, *TP53* missense mutations, CNVs, mRNAs and protein expression values were examined from the cBioPortal. It was observed that *TP53* mRNA and protein were significantly increased in LUAD and lung squamous cell carcinoma (LUSC) tissues compared to adjacent normal tissues (Figures 2A and 2B). In LUADs particularly, the mRNA level was not altered between wild-type and missense mutation cases (Figure 2C), although a significant difference existed between CNV amplification and deletion groups (Figure 2D). An interesting finding was that p53 protein level was significantly higher in missense mutation cases (Figure 2E) independent of CNV status (Figure 2F), suggesting that the upregulation of p53 in missense cases is derived from post-transcription in LUAD. In contrast, LUSC samples exhibited significantly higher *TP53* mRNA and p53 protein levels in missense mutation cases

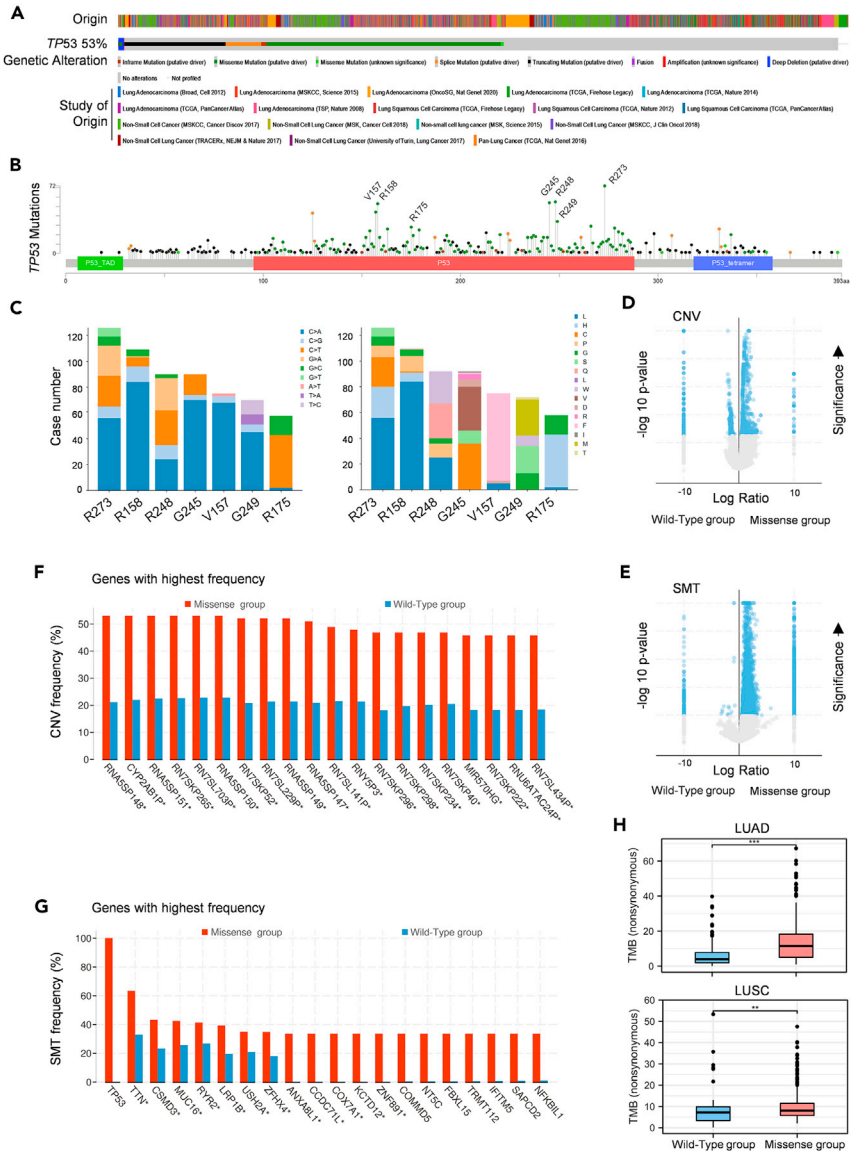

Figure 1. TP53 mutations are correlated with chromosomal instability and tumor mutation burden in non-small cell lung cancers (NSCLCs)

(A) General mutant frequency of TP53 originated from 17 NSCLCs studies. Specific colors indicate TP53 genetic alternatives.

(B) Distribution of p53 missense mutations according to the sequence of p53 protein.

(C) Histogram indicating the constituent 6 hotspot missense mutations derived from nucleotide alteration (left) and amino acid substitution (right).

(D) Volcano plot indicating log ratio of copy number variation (CNV) frequency between TP53 wild-type and missense mutation groups (q value < 0.05).

(E) Volcano plot indicating log ratio of somatic mutation (SMT) frequency between TP53 wild-type and missense mutation groups (q value < 0.05).

(F) Histogram showing the top 20 genes with highest CNV frequency.

(G) Histogram showing the top 20 genes with highest SMT frequency.

(H) The tumor mutation burden (TMB) of non-synonymous mutations between TP53 wild-type and missense mutation groups in LUAD and LUSC (TCGA, Pan Cancer Atlas) (Wilcoxon rank-sum test, **p < 0.01, ***p < 0.001). The boxes indicated the median ± 1 quartile, the whiskers extended to the farthest non-outliers within 1.5 × IQR from the box boundaries, outliers were also marked.

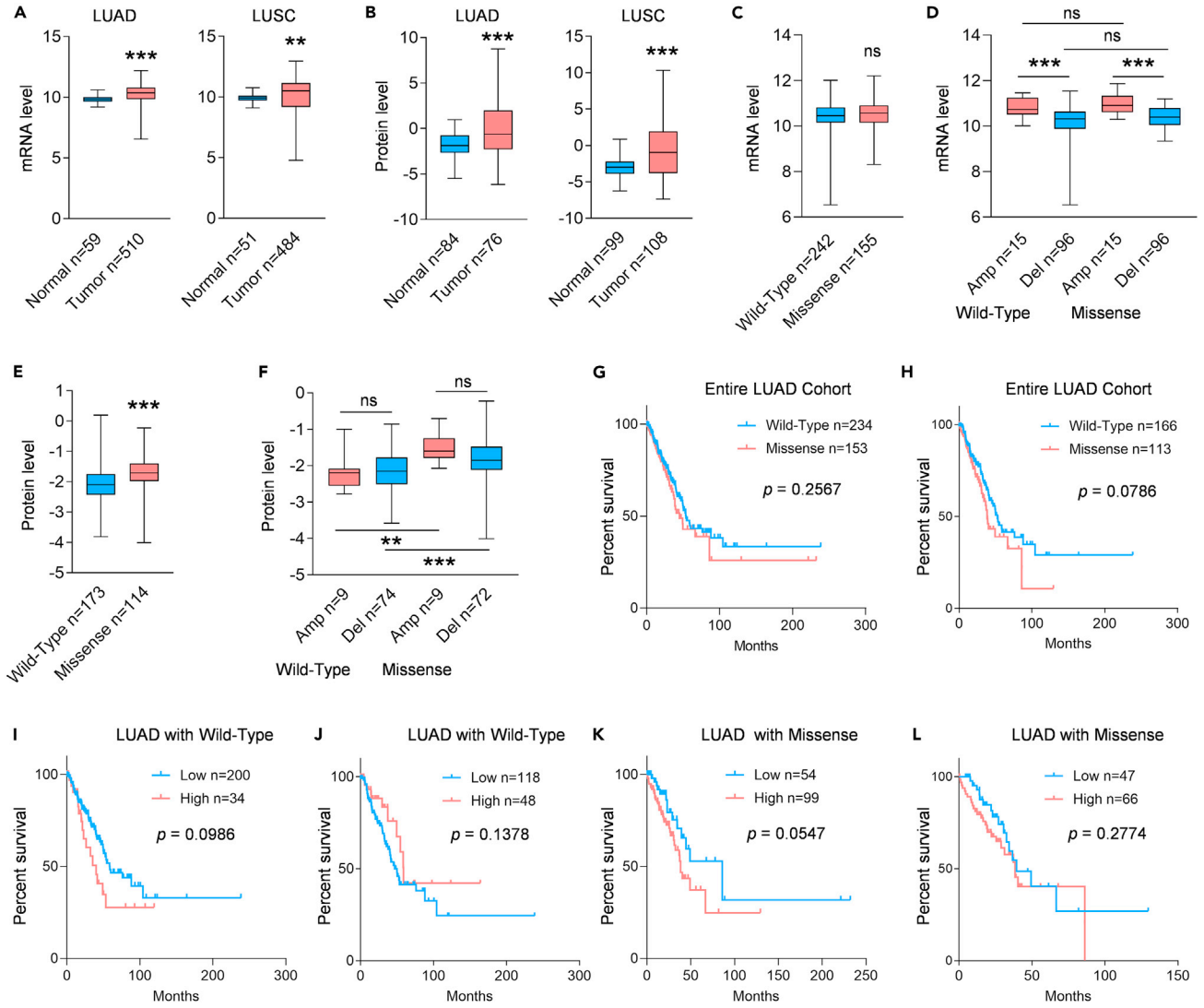

Figure 2. Missense mutations correlated with higher p53 protein expression predict poor survival in NSCLCs

(A) Analysis of TP53 mRNA expression between normal and tumor samples in lung adenocarcinoma (LUAD) or lung squamous cell carcinoma (LUSC) (Wilcoxon rank-sum test, **p < 0.01, ***p < 0.001).

(B) Analysis of p53 protein levels between normal and tumor samples in LUAD or LUSC (LUAD: Wilcoxon rank-sum test; LUSC: unpaired Student's *t* test, ***p < 0.001).

(C) Analysis of TP53 mRNA expression between wild-type and missense mutant groups in LUADs (Wilcoxon rank-sum test).

(D) Pairwise comparison of TP53 mRNA expression between wild-type and missense mutant groups in LUADs grouped by copy number variations (Amp, amplification; Del, deletion) (unpaired Student's *t* test was used to compare the differences between "wild-type Amp n = 15" and "missense Amp n = 15", Wilcoxon rank-sum test was applied for the remaining groups; ns, no significance, ***p < 0.001).

(E) Analysis of p53 protein expression between wild-type and missense mutant groups in LUADs (Wilcoxon rank-sum test, ***p < 0.001).

(F) Pairwise comparison of p53 protein expression between wild-type and missense mutant groups in LUADs grouped by copy number variations (Wilcoxon rank-sum test, ns, no significance, **p < 0.01, ***p < 0.001).

(G, I, K) Kaplan-Meier curves showing overall survival of patients in the indicated LUAD cohorts based on RNA-seq data guided by TP53 optimal cutoff value (Log rank, p values indicated).

(H, J, L) Kaplan-Meier curves showing overall survival of patients in the indicated LUAD cohorts based on protein data guided by p53 optimal cutoff value (Log rank, p values indicated).

For these boxplots, the boxes represented the median ±1 quartile, while the whiskers extending from the top and bottom sides reach the maximum or minimum value.

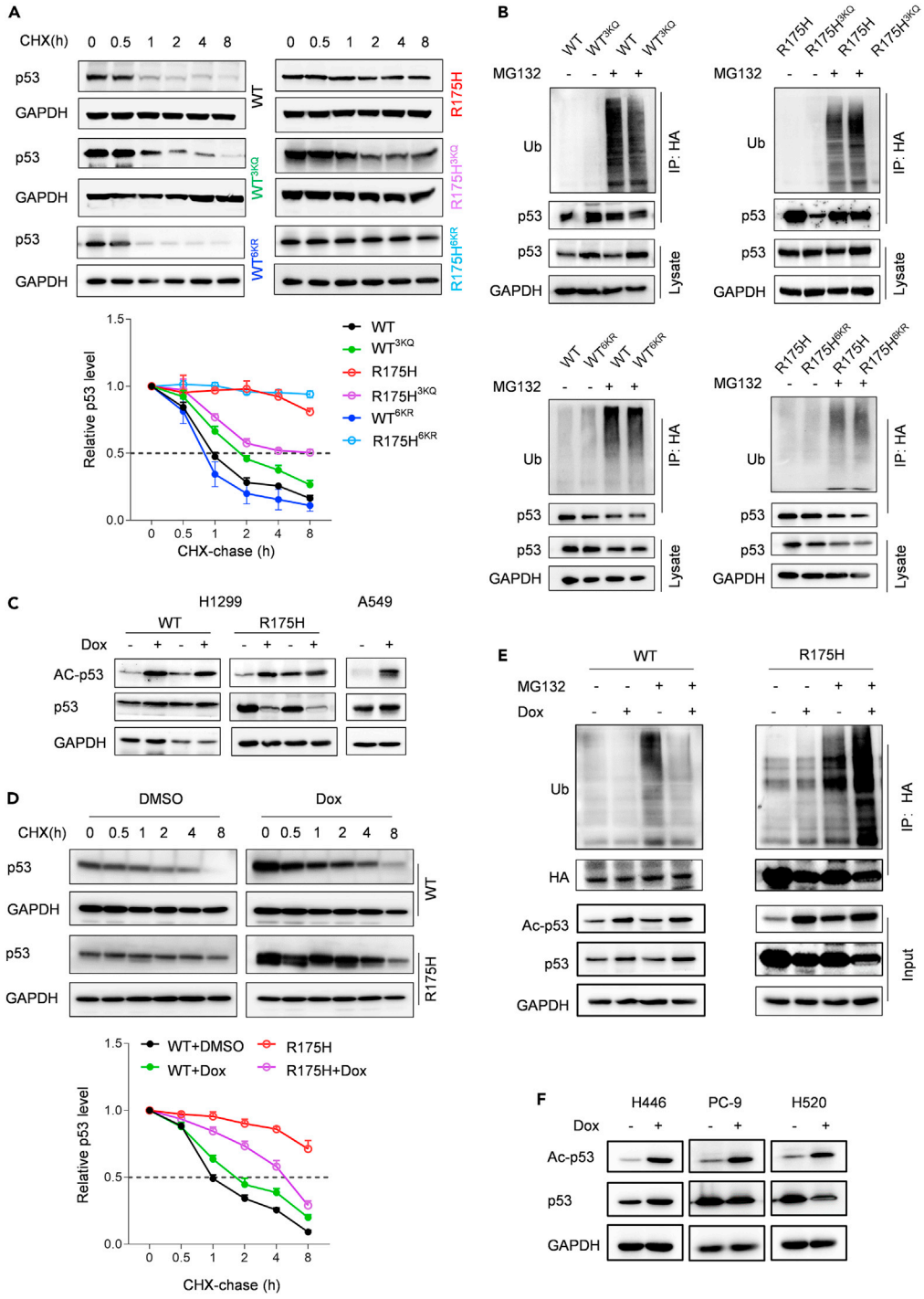

Figure 3. Acetylation promotes wild-type p53 stability, but drives missense mutant p53 ubiquitination and degradation

(A) Western blot analysis detected the expression of p53 in H1299 cells treated with cycloheximide (CHX; 20 μg/mL) for the indicated times. The trend of p53 alterations are shown (mean ± SD and determined using Student's t tests, n = 3).

(B) Ubiquitination assay of the indicated p53 constructs in H1299 cells. Cells were incubated with MG132 (20 μM) for 6 h before harvest. Ubiquitin (Ub)-binding p53 was immunoprecipitated (IP) by HA antibody and detected by Ub antibody. Target proteins in the total lysate were detected using indicated antibodies.

(C) Western blot analysis indicated the expression of p53 and acetylated p53 in the indicated cells treated with or without doxorubicin (Dox; 1 μM) for 2 h.

Figure 3. *Continued*

(D) Western blot analysis detected p53 stability in H1299 cells treated with Dox (1 μM) and CHX (20 μg/mL) for the indicated times. The trend of p53 alterations was shown (mean ± SD and determined using Student's t tests, n = 3).

(E) Ubiquitination assay of p53 in H1299 cells expressing the indicated constructs. Cells were treated with or without Dox (1 μM) for 2 h and incubated with MG132 (20 μM) for 2 h before harvest.

(F) Western blot analysis of total p53 and acetylation in NSCLC cell lines treated with or without Dox (1 μM) for 2 h.

(Figures S1A–S1D). Subsequently, survival analysis and relative risk of death (hazard ratio, HR) were applied to explore the clinical relevance of the *TP53* gene status. In the entire LUAD cohort, the overall survival was independent of mRNA level of *TP53* wild-type or missense mutation (Figure 2G). At the protein level, although no significant difference was found, patients with p53 missense mutation have a certain worse survival probability (Figure 2H). Guided by the optimal cutoff value calculated by X-Tile, we further analyzed the survival outcomes in reference to the expression of *TP53*/p53 wild-type or missense mutation. As shown in Figures 2I and 2J and Table S4, lower levels of wild-type p53 mRNA were associated with a reduced death risk and predicted a relative better survival outcome, while no significant difference was observed at protein level in wild-type p53 cases. For p53 missense mutant patients, the survival analysis showed the results similar to those of wild-type p53 containing patients (Figures 2K and 2L). In LUSC cohort, an interesting finding was that p53 missense mutation predicted a promising survival outcome both at mRNA and protein (Figures S1E and S1F). Ultimately, according to the optimal cutoff value grouping rule, the expression of wild-type or missense mutated p53 mRNA and protein had no clinical significance (Figures S1G–S1J). Collectively, these results reveal that p53 missense mutations are not necessarily associated with adverse outcomes in NSCLCs.

Acetylation promotes wild-type p53 stability, but drives missense mutant p53 ubiquitination and degradation

Missense mutant p53 bears functional consequences that are distinct from the wild-type protein.[28] Therefore, the regulation of missense mutant p53 at protein level in NSCLCs deserves further attention. The upregulation of missense mutated p53 at the protein level independent of mRNA was recurrent in an NSCLC cell line (Figures S2A and S2B), indicating that post-transcriptional regulation is an important mechanisms regulating the activity and stability of wild-type and mutant p53 in NSCLCs.[29] Since acetylation is crucial for p53 stability and functional execution, we explored whether acetylation exerts differential effects on the stability of wild-type (WT) and missense mutant p53. Here, a common structural mutation, R175H, was introduced into the following experiments. Acetylation of the CTD is a determinant of p53 DNA binding and tumor suppressing properties.[30] Current knowledge suggests that CTD acetylation occurs at six lysine sites covering K370, 372, 373, 381, 382, and 386. Given that the stability of p53 is mainly regulated by acetylation of CTD, the CTD constitutive acetylation mutant (3KQ), in which lysine (K) was converted to glutamine (Q) at K373, K381, and K382, and the CTD non-acetylation mutant (6KR), in which the six known CTD acetylation sites were converted to arginine (R), were used for subsequent study (Figure S3A). With these constructs, the stable cell lines expressing Mock, wild-type p53 (WT), WT 3KQ (WT^{3KQ}), R175H, R175H 3KQ ($R175H^{3KQ}$), WT 6KR (WT^{6KR}), and R175H 6KR ($R175H^{6KR}$) were established in H1299 cells, a p53-null NSCLC cell line (Figure S3B). With these constructs, the effects of acetylation on p53 protein stability were determined by the cycloheximide (CHX) chase analysis. It was observed that wild-type p53 was a short-lived protein with a half-life of about 1 h, while the half-life of R175H was markedly prolonged, and no significant degradation was observed during the observation period (Figure 3A). These findings are consistent with results derived from a bioinformatics analysis demonstrating that the level of missense mutant p53 was significantly higher than that of wild-type p53. As expected, simulated acetylation (WT^{3KQ}) increased the half-life of p53 from 1 h to nearly 2 h, confirming that acetylation enhances p53 stability.[30] However, a surprising observation was that $R175H^{3KQ}$ underwent a faster degradation than R175H, suggesting that acetylation impairs the stability of R175H. For the non-acetylation mutants, there were no significant alterations in stability were found in WT^{6KR} and $R175H^{6KR}$compared to their respective non-lysine mutated constructs (Figure 3A). Moreover, ubiquitin experiments indicated that acetylation resulted in a reduction in the ubiquitination of wild-type p53, but induced an increase in the ubiquitination of R175H (Figure 3B, above). Consistent with a previous report that CTD 6KR mutation has no effect on p53 stability,[31] there was no obvious difference of ubiquitination observed between WT and WT^{6KR}, as well as between R175H and $R175H^{6KR}$ (Figure 3B, below). This suggests that CTD acetylation is a crucial protein modification for both wild-type and mutant p53, but with opposite effects. To further confirm these findings, we deployed doxorubicin (Dox) as an acetylation inducer.[32,33] As shown in Figure 3C, Dox chase induced acetylation of endogenous wild-type p53 and increased overall p53 levels in A549 cells. The acetylation and

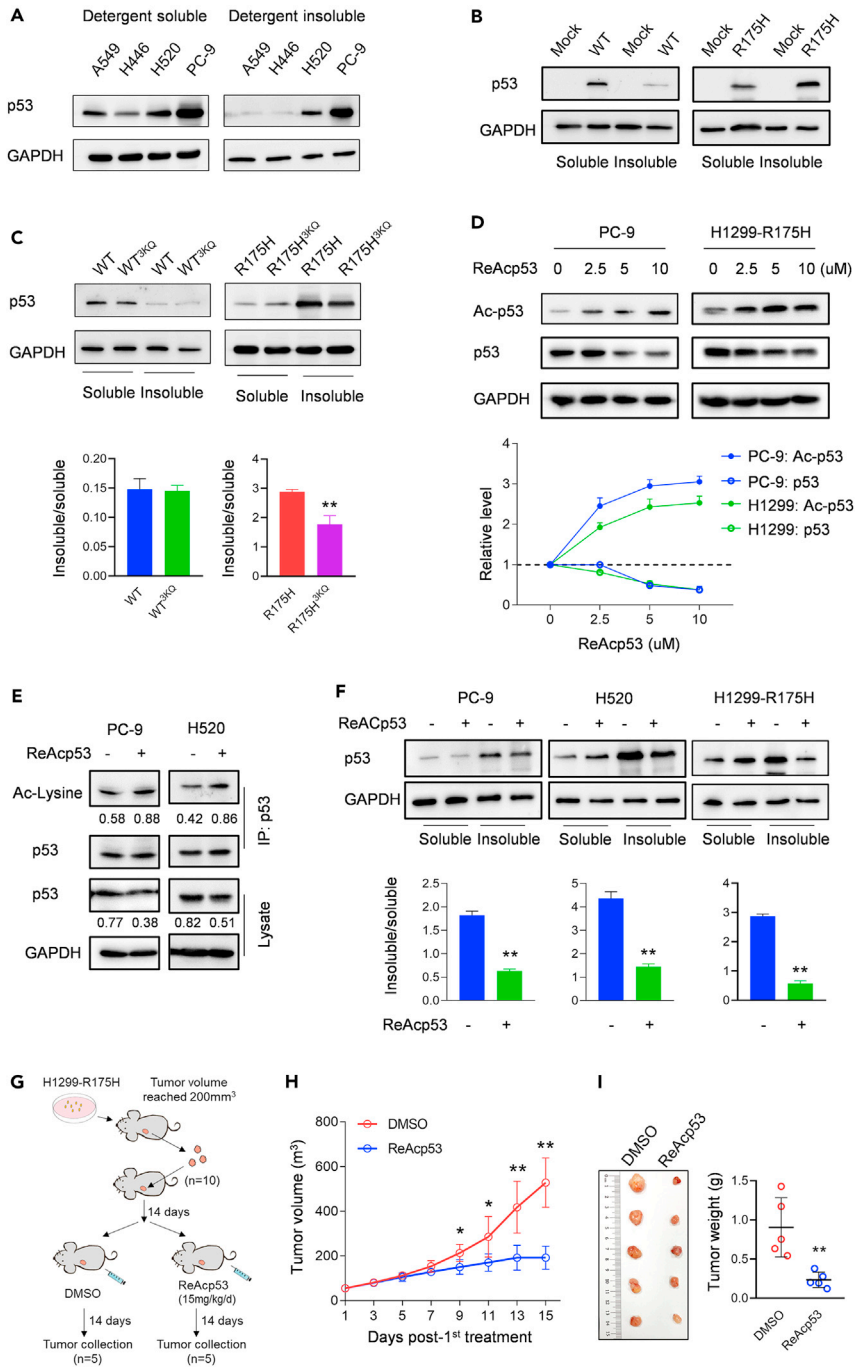

Figure 4. Acetylation halts aggregation and reactivates missense mutant p53

(A) Western blot analysis detected the solubility of p53 in indicated NSCLC cells. GAPDH served as a loading control.

(B) Western blot analysis showed the solubility of ectopic p53 and R175H in H1299 cells.

(C) Western blot analysis detected the effect of acetylation simulation on p53 solubility. The lower panel showed the quantitative of solubility ratio between the indicated groups (mean ± SD and determined using Student's t tests, n = 3, $^{**}p < 0.01$).

(D) Western blot assay demonstrated the expression of p53 and acetylated p53 in the indicated cells treated with increased concentrations of ReAcp53 for 20 h. The lower panel displays the trend of the indicated protein alteration. Data were expressed as mean ± SD.

(E) IP analysis detected the overall p53 acetylation in the indicated cells treated with ReAcp53 (5 μM) for 20 h. Cell lysates were obtained by IP using p53 antibody followed by Western blot assay using the indicated antibodies.

Figure 4. *Continued*

(F) Western blot analysis detected the effect of ReAcp53 on p53 solubility in the indicated cells treated with ReAcp53 (5 μM) for 20 h. The lower panel shows the quantitative solubility ratio between the indicated groups (mean ± SD and determined using Student's t tests, n = 3, **p < 0.01).

(G) Schematic illustration of the evaluation of *in vivo* tumor growth derived from H1299-R175H cells responding to ReAcp53 treatment. Mice bearing tumors with volume of 200 m3 were randomly grouped and received intraperitoneal injections of DMSO or ReAcp53 (15 mg/kg) every day for 14 days. Tumor volume was monitored as indicated from the first treatment. Tumors were collected on the 15th day post-first treatment.

(H) Growth curve of subcutaneous xenografts. (Mean ± SD and determined using Student's t tests, n = 5, *p < 0.05, **p < 0.01).

(I) Representative images of subcutaneous xenografts collected at the 15th day after first treatment. The right panel shows the tumor weight statistics (mean ± SD and determined using Student's t tests, n = 5, **p < 0.01).

expression induced by Dox treatment also occurred in ectopic wild-type p53, but Dox treatment achieved contrary results on acetylation status and overall expression of R175H. CHX chase analysis indicated that Dox promoted the half-life of wild-type p53 and accelerated the degradation of R175H (Figure 3D), confirmed by ubiquitin experiments (Figure 3E). The adverse effect of Dox intervention on the stability of wild-type and mutant p53 was subsequently verified in NSCLC cells expressing endogenous p53. (Figure 3F). Collectively, these data reveals that acetylation exerts diametrically opposed effects on wild-type and mutant p53 in NSCLC cells.

Acetylation halts aggregation and reactivates missense mutant p53

The stability of mutant p53 is due to aggregation, and restoring solubility can rescue tumor suppression.[34–36] Western blot detection of detergent-soluble and insoluble fractions derived from NSCLC cell lines covering wild-type (A549, H446) and missense mutant p53 (H520 with W146Q, PC-9 with R248Q) showed that most of wild-type p53 exists in soluble components, while a considerable part of missense mutant p53 was detected in detergent insoluble components (Figure 4A). The detection in H1299 cells expressing ectopic p53 further confirmed these findings (Figure 4B). In acetylation simulation experiments, it was found that acetylation did not affect the distribution of wild-type p53 across soluble or insoluble components, however, an increase of R175H in the soluble component was observed (Figure 4C). This evidence suggests that acetylation promotes the solubility of mutant p53, while the stability of wild-type p53 is not affected by increased insolubility. Halting aggregation or increasing solubility may rescue missense mutated p53 transcriptional regulation.[34] To explore this in our model, a p53 luciferase reporter assay was applied to evaluate whether acetylation contributes to p53 mutant reactivation. As shown in Figure S4A, wild-type p53 introduction endows significant p53 transcriptional activity in p53 null-H1299 cells and acetylation simulation further promotes the induction of wild-type p53. The activity of p53 in R175H expressing cells was comparable to control H1299 cells, indicating that mutant p53 does not possess p53 transcriptional activity. Acetylation stimulation re-endowed p53 transcriptional activity in R175H mutant mimics. Transcriptome sequencing was further used to determine the expression of p53 across the various constructs in H1299 cells. Gene set enrichment analysis (GSEA) indicated that WT and R175H expression in H1299 cells reproduced the enrichment results from the NSCLC cohort, embodied in genes involved in the p53 pathway, G2M checkpoint, TGFβ signaling, Notch signaling, etc. (Figure S4B). Further analysis illustrated enhanced p53 pathway enrichment induced by p53 acetylation, but also indicated loss of p53 pathway regulation in R175H-expressing cells (Figure S4C). To determine whether 3KQ confers direct transcriptional or DNA-binding ability to R175H p53, qPCR was performed to detect the expression of p53-targeted genes regulating apoptosis in cells treated with Dox. As shown in Figure S4D, Dox induced an increase of p53-targeted genes in $R175H^{3KQ}$ cells but failed to regulate these genes in R175H cells. ChIP-qPCR assay indicated that Dox significantly promoted p53 binding to the targeted promoters in $R175H^{3KQ}$ cells, whereas no detectable p53 DNA-binding promotion was found in Dox treated R175H cells (Figure S4E). Their findings suggest that acetylation directly rescues the p53 transcriptional activity of R175H, restoring p53 functional and pathway regulation. Therefore, acetylation stimulation restores mutant P53 by connecting structural and chemical alterations and promoting solubility.[37] Subsequently, ReACp53, a p53 activator targeting p53 aggregation,[34] was applied to evaluate the correlation between acetylation and solubility of mutant p53. PC-9 cells containing R248Q and H1299 cells expressing R175H were simultaneously treated with gradient concentrations of ReAcp53 for 20 h (Figure 4D). ReAcp53 treatment resulted in a concentration-dependent increase of p53 acetylation. Using an antibody targeting acetylated lysine (Ac-lysine), IP analysis further showed that ReAcp53 induced p53 acetylation in cells containing endogenous missense mutated p53 (Figure 4E). Accordingly, ReAcp53 treatment induced

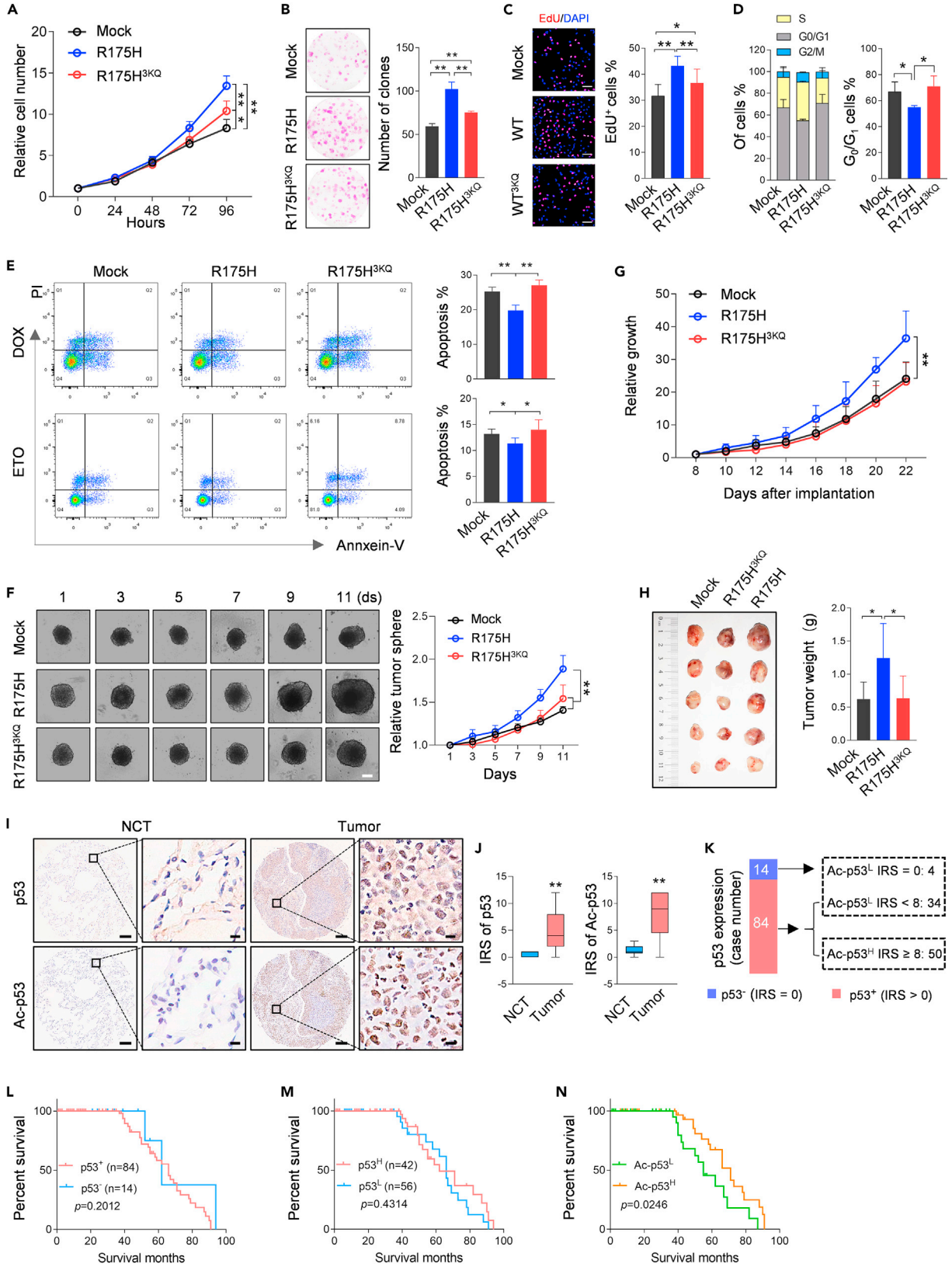
A
Mock
R175H
R175H3KQ
Relative cell number
Hours
B
Mock
R175H
R175H3KQ
Number of clones
C
EdU/DAPI
Mock
WT
WT3KQ
EdU+ cells %
D
S
G0/G1
G2/M
Of cells %
G0/G1 cells %
E
Mock
R175H
R175H3KQ
PI
DOX
ETO
Annxein-V
Apoptosis %
G
Relative growth
Days after implantation
F
1
3
5
7
9
11 (ds)
Relative tumor sphere
Days
H
Tumor weight (g)
I
NCT
Tumor
p53
Ac-p53
J
IRS of p53
IRS of Ac-p53
K
p53 expression (case number)
14
84
Ac-p53L IRS = 0: 4
Ac-p53L IRS < 8: 34
Ac-p53H IRS ≥ 8: 50
p53- (IRS = 0)
p53+ (IRS > 0)
L
Percent survival
p53+ (n=84)
p53- (n=14)
p=0.2012
Survival months
M
p53H (n=42)
p53L (n=56)
p=0.4314
N
Ac-p53L
Ac-p53H
p=0.0246

Figure 5. Acetylation reverses p53 missense mutation gain-of-functions and rescues tumor suppressive activity

(A) Cell growth assay of H1299 cells expressing the indicated constructs (mean ± SD and determined using one-way analysis of variance, n = 6, *p < 0.05, **p < 0.01).

(B) Colony formation assay of H1299 cells (mean ± SD and one-way analysis of variance, n = 3, **p < 0.01).

(C) EdU incorporation assay detecting the DNA replication of H1299 cells (mean ± SD and one-way analysis of variance, *p < 0.05, **p < 0.01). Data were expressed as the percentage of EdU positive cells (Red) to total Hoechst-labeled cells (Blue). Bars, 20 μM.

(D) Cell cycle detection by flow cytometry and the statistical results (mean ± SD and one-way analysis of variance, n = 3, *p < 0.05).

(E) Apoptosis assay of H1299 cells. Cells were treated with Dox (0.5 μM) and Eto (10 μM) for 24h and apoptotic cells were analyzed by flow cytometry (mean ± SD and one-way analysis of variance, n = 3, *p < 0.05, **p < 0.01).

(F) Representative images of 3D-spheroid growth assay (left) and statistics (right; mean ± SD and one-way analysis of variance, n = 5, **p < 0.01). Bars, 500 μM.

(G) Growth curve of subcutaneous xenografts derived from H1299 cells. The tumor volume was measured at the indicated times after implantation (mean ± SD and one-way analysis of variance, n = 5, **p < 0.01).

(H) Representative images of subcutaneous xenografts collected at the 22nd day after implantation. The right panel shows the tumor weight statistics (mean ± SD and one-way analysis of variance, n = 5, **p < 0.05).

(I) Representative images of p53 and Ac-p53 IHC in non-cancerous tissues (NCT) and LUADs (tumor) tissues. Scale bars, 200 μm in whole images and 10 μm in local enlarged images.

(J) Immunoreactivity scoring (IRS) analysis of p53 and Ac-p53 expression (mean ± SD and determined using Student's t tests, **p < 0.01).

(K) Diagram showing high (Ac-p53H) and low Ac-p53 (Ac-p53L).

(L) Overall survival analysis grouped by p53 positive and negative tissues (Log rank).

(M) Overall survival analysis grouped by high p53 and low p53 based on IRS cutoff of 6 (Log rank).

(N) Overall survival analysis grouped by high Ac-p53 and low Ac-p53 based on IRS cutoff of 8 (Log rank).

enhancement of endogenous or ectopic missense mutant p53 solubility (Figure 4F) and, not surprisingly, significantly inhibited growth of tumors derived from H1299 cells expressing R175H (Figures 4G–4I). Collectively, the evidence points to a mechanism whereby acetylation halts aggregation and enhances the solubility of missense mutated p53, thus rescuing p53 pathway regulation.

Acetylation reverses p53 missense mutation gain-of-function and rescues tumor suppressor activity

It is widely believed that missense mutant p53 leads to a dominant gain-of-function that result in genomic instability that belies malignant cancer cell phenotypes.[38] The introduction of R175H promoted cell growth, colony formation, and DNA replication in H1299 cells (Figures 5A–5C). Cell cycle analysis showed that R175H expression resulted in a decrease of cells in the G0/G1 phase and a concomitant increase in cells in G2/M phases (Figure 5D). R175H expression also protected cell from apoptosis induced by Dox or ETO (Figure 5E), confirming the established view that mutant p53 blunts the tumor cell's response to chemotherapy.[39] This gain-of-function was documented in R175H-expressing, p53-null H1299 cells. To confirm that acetylation reverses the GOF of missense mutant p53,[26,40] the functions of $R175H^{3KQ}$ in H1299 cells were also examined. As shown in Figures 5A–5C, $R175H^{3KQ}$ partly impaired the GOF of R175H regarding cell proliferation. Moreover, acetylation induced R175H-specific loss of GOF cell cycle dynamics (Figure 5D) and anti-apoptosis (Figure 5E). Furthermore, 3D-spheroid growth assay (Figure 5F) and subcutaneous xenograft growth assay (Figures 5G and 5H) indicated that R175H expression resulted in significant tumor growth promotion *in vitro* and *in vivo*. While $R175H^{3KQ}$-expressing cells exhibited comparable tumorigenesis and growth in Mock-expressing cells, disclosing acetylation completely reversed the tumor promotion of missense mutant p53. To determine the significance of p53 acetylation in NSCLCs, a human primary NSCLC tissue microarray (including 98 tumor samples and 82 NCT) was performed using p53 or acetylated p53 (acetyl K382) antibodies (Figure 5I). The sections used for p53 and acetylated p53 were adjacent. Results showed that the expression of p53 and acetylated p53 were extremely low in NCTs but significantly upregulated in tumor tissues (Figures 5I and 5J). p53 and acetylated p53 were mostly notably expressed in cellular nuclei. Immunohistochemical (IHC) quantification showed 84 tumor samples expressed p53 ($p53^{+}$) and 14 samples did not express p53 ($p53^{-}$) (Figure 5K). After excluding for p53 negative cases positive for acetylated p53, a total of 50 cases of highly acetylated p53 ($Ac\text{-}p53^{H}$) and 38 cases of lowly acetylated p53 ($Ac\text{-}p53^{L}$) remained, based on the IRS cutoff value of 8. The overall survival analysis indicated no significant difference between patients with p53 positive and negative (Figure 5L) histology, nor between patients with high or low p53 expression based on the IRS cutoff of 6 (Figure 5M), suggesting that p53 expression independently holds no predictive value for NSCLC patients. For acetylated p53, those with higher acetylation did observe better predicted survival outcomes (Figure 5N). Collectively, these observations reveal that acetylation can reverse the dominant, GOF of common p53 missense mutants and predicts improved outcomes of NSCLC patients.

DISCUSSION

The prevalence of p53 mutations, subsequent structural and oncogenic functions suggest a potential for p53 mutations as an indicator of patient outcomes, while little to no evidence supports the independent prognostic capacity of *TP53* expression and mutation status in NSCLCs.[41,42] Additionally, how *TP53* mutations contribute to tumor progression is not resolved. Kennedy and Lowe outline three mutant *TP53* mechanisms, including loss of p53 functions, dominant inhibition of p53 functions, and gain of oncogenic functions of mutant p53 products.[43] Unraveling these mechanisms in NSCLC patients are essential to improve categorization and treatment of *TP53* mutant tumors. It was posited that one of the requirements for mutant p53's gain of oncogenic functions involves post-transcriptional modifications, such as escape from MDM2-specific ubiquitination, the dominant negative regulator of p53, and allowing abnormal accumulation in mutant p53-expressing cancer cells.[20,44,45] However, the post-transcriptional dynamic has not been fully demonstrated in mutant p53. Thus, this study aimed to address the relationship between p53 missense mutations, acetylation/ubiquitination dynamics, downstream regulatory processes, and patient survival with NSCLC tumors. Moreover, we sought to reconcile the mechanism of acetylation with the observed pro-oncogenic roles of missense mutant p53.

We report that missense *TP53* mutations accounted for 65% of all p53 mutations, mostly occurring in the DBD, in line with previous assessments of *TP53* missense mutations in TCGA lung cancer patients.[46] Missense mutant p53 samples were highly correlated with chromosomal instability as demonstrated by their higher rates of TMB, consistent to the previous observations in NSCLC cohorts.[47,48] *TP53* mRNA and protein were elevated in LUAD and LUSC tissues, though the contribution of missense mutations was not straightforward. In LUADs, p53 protein appeared to be altered post-transcriptionally in missense mutation cases, while in LUSCs, the increase appeared related to elevated *TP53* mRNA. Neither mRNA nor p53 protein were adequate predictors of survival in the LUAD cohort. In LUSC cases, increased expression of p53 (mRNA and protein) missense mutations was correlated with improved survival, though not clinically significant. These results suggest that the presence of p53 missense mutations is not rooted with adverse survival outcomes in NSCLCs, in line with the proposal that not all p53 missense mutations were "disruptive",[49] though the stratification of disruptive versus non-disruptive p53 mutations has not identified successful. It does stand to reason that toward a unifying strategy for the adoption of a p53 mutation prognostic, much is left to understand about the breadth and scope of p53 mutations in NSCLCs.

The upregulation of missense mutant p53 at the protein level, independent of mRNA, was recurrent in an NSCLC cell line, implying that a post-transcriptional mechanism regulates the elevation of mutant p53 protein. We found that acetylation increases the half-life/stability of WT p53 but accelerates the degradation of the structural, missense "hotspot" mutant R175H. This diametrically opposed action is concurrent with the known competitive inhibition of acetylation/ubiquitin and the MDM2/ubiquitin-independent pathways of mutant p53s, including R175H.[50] Histone deacetylase (HDAC) inhibitor releases the degradation protection mechanism of mutant p53 and strongly chemosensitizes mutant p53 cancer cells.[51] Present findings provide directly evidence that acetylation promotes the ubiquitination degradation, and endows normative p53 functionality by acetylation/solubility of mutant p53. Similarly restored tumor suppression have been observed by designer peptides and small stress molecules aimed at de-aggregating/correcting protein misfolding of mutant p53.[34,35,52,53] The current evidence that acetylation promotes solubility of R175H suggests a possibility that acetylation modifies or orders the secondary structure and folding of missense mutant p53, thus partially restoring p53 functions, including DNA-binding capacity. In view of the perquisite of missense mutant p53 accumulation for gain of oncogenic functions, these findings bear significant implications that de-aggregation of mutant p53 could rescue tumor suppression. Treatment of R175H-expressing cells with the designer peptide ReACp53 simultaneously increased acetylation and solubility of mutant p53, prompting the need for further investigation of the hierarchy of acetylation and the structural dynamics that render mutant p53 aggregation.[37,51,54] These may even be further complicated by the disease stage and tissue type. Ultimately, refining our understanding of the structural and molecular landscape of one specific p53 mutation in a cancer-specific context may be the first step to unraveling the diverse regulation of mutant p53.

This study adopted a multi-faceted approach, leveraging clinical data repositories and bioinformatics tools in tandem with precision cellular constructs for mechanistic understanding. Our view of the inquisition of mutant TP53 acetylation allowed for more in-depth answers than what were previously available for NSCLC. A thorough understanding of the post-transcriptional modulation of missense mutant p53 is

critical for the precise and clinical use of TP53 mutations as prognostic indicators or even diagnostic tools in the future. Some improvements include expanding our scope to other missense mutation "hotspots" in order to confirm or broaden the findings among other common p53 missense mutations. For example, R273 contributes 5% of NSCLC mutations and has also been observed to possess gain of oncogenic functions.[28] Additionally, focusing on MMD2/ubiquitin-independent stability dynamics due to the known existence of E3 ligase-evading TP53 missense mutations.[55] Finally, determining ground-truth accuracy of survival predictions based on more complex p53 mutation stratifications with longitudinal, prospective studies.

Missense p53 mutant acetylation status bears significant weight on the aggregation/insolubility of the p53 mutant, in turn directing E3 ligase degradation and/or cytoplasmic sequestration. Importantly, constitutive acetylation demonstrated a restoration of tumor suppressor function, rescuing gain of oncogenic function phenotypes comparable to designer peptides. Thus, we conclude that acetylation negatively regulates mutant p53 by targeting aggregation/stability dynamics and inhibiting the gain of oncogenic functions required for tumor growth. Acetylation inducer targeting mutant p53 is thus, a novel therapeutic target for NSCLCs and may improve accuracy of current efforts to utilize p53 mutation status as a prognostic.

Limitations of study

In this study, it would be better to use naturally occurring acetylation or deacetylation instead of construct mutant, to eliminate the potential effects caused by ectopic expression.

To verify the effect of acetylation on wild-type and missense mutant p53, only R175H mutation was introduced into functional experiments, which may not be representative of all missense mutation features.

The study does not reveal possible mechanism to distinguish between wild-type and missense mutant p53 stability regulated by acetylation.

ETHICS STATEMENT

The study was approved by the Institutional Ethics Committee of Wuxi People's Hospital of Nanjing Medical University.

STAR★METHODS

Detailed methods are provided in the online version of this paper and include the following:

- KEY RESOURCES TABLE
- RESOURCE AVAILABILITY
  - Lead contact
  - Materials availability
  - Data and code availability
- EXPERIMENTAL MODEL AND SUBJECT DETAILS
  - Cell lines
  - Clinical sample and immunohistochemical staining
  - Tumor xenografts in nude mice
- METHOD DETAILS
  - Online cancer database acquisition and analysis
  - Gene enrichment assay
  - Vector construction and transduction
  - Western blot assay
  - Immunoprecipitation (IP) assays
  - p53 transcriptional reporter assay
  - Transcriptome sequencing and data analysis
  - Cell growth and colony formation assay
  - Cell cycle assay
  - EdU incorporation assay
  - 3D-spheroid formation and growth measurement
  - Cell apoptosis analysis
  - Reverse-transcription quantitative PCR (RT-qPCR)
  - ChIP and ChIP-qPCR assays

- QUANTIFICATION AND STATISTICAL ANALYSIS
- ADDITIONAL RESOURCES

SUPPLEMENTAL INFORMATION

Supplemental information can be found online at https://doi.org/10.1016/j.isci.2023.107003.

ACKNOWLEDGMENTS

This work was supported by Natural Science Foundation of China (NFSC) grants (no. 82172954, 81903391, 81872056, 81802493, 82003581, and 82203757), Natural Science Foundation of Jiangsu Province (BK20190148 , BK20220225), "333" Engineering Project Jiangsu Province ([2022] 2-060), Jiangsu Young Medical Talents (QNRC2016188), Wuxi Key Medical Talents (ZDRC001), Wuxi Commission of Health Precision Medicine Special Funds (J201803), Wuxi Science and Technology Development Fund (N20192048), Taihu Talent Plan (JZ), Reserve Talents of Double Hundred Talent Plan (HB2020017, HB2020018), General Program of Jiangsu Commission of Health (M2020012), Wuxi Translational Medicine Research Project (2020ZHZD04). We thank Clarity Manuscript Consultants for assistance with language editing (www.clarity-manuscripts.com/about.html).

AUTHOR CONTRIBUTIONS

All authors read the manuscript and provided feedback. D.X.X., W.Q., Z.H.Z., Z.K.Y., and P.S. conducted experiments, acquired, and analyzed data. Z.K.Y., W.Q., Y.Y., Y.L.H., L.L.G., B.Z., X.S.Y., P.H.L. conducted experiments and acquired data. Z.N.P. and P.H.L. analyzed data. D.X.X., W.Q., Z.N.P., and J.Z. edited the manuscript. Z.N.P. and J.Z. designed the research.

DECLARATION OF INTERESTS

The authors have declared that no conflict of interest exists.

INCLUSION AND DIVERSITY

We support inclusive, diverse, and equitable conduct of research.

Received: February 13, 2023
Revised: April 28, 2023
Accepted: May 26, 2023
Published: May 30, 2023

REFERENCES

1. Boutelle, A.M., and Attardi, L.D. (2021). p53 and tumor suppression: it takes a network. Trends Cell Biol. *31*, 298–310. https://doi.org/10.1016/j.tcb.2020.12.011.

2. Donehower, L.A., Soussi, T., Korkut, A., Liu, Y., Schultz, A., Cardenas, M., Li, X., Babur, O., Hsu, T.K., Lichtarge, O., et al. (2019). Integrated analysis of TP53 gene and pathway alterations in the cancer genome Atlas. Cell Rep. *28*, 1384–3010.e5. https://doi.org/10.1016/j.celrep.2019.08.061.

3. Weisz, L., Zalcenstein, A., Stambolsky, P., Cohen, Y., Goldfinger, N., Oren, M., and Rotter, V. (2019). Retraction: transactivation of the gene contributes to mutant p53 gain of function. Cancer Res. *79*, 2085. https://doi.org/10.1158/0008-5472.Can-19-0560.

4. Scian, M.J., Stagliano, K.E., Anderson, M.A., Hassan, S., Bowman, M., Miles, M.F., Deb, S.P., and Deb, S. (2005). Tumor-derived p53 mutants induce NF-kappaB2 gene expression. Mol. Cell Biol. *25*, 10097–10110. https://doi.org/10.1128/MCB.25.22.10097-10110.2005.

5. Suh, Y.A., Post, S.M., Elizondo-Fraire, A.C., Maccio, D.R., Jackson, J.G., El-Naggar, A.K., Van Pelt, C., Terzian, T., and Lozano, G. (2011). Multiple stress signals activate mutant p53 in vivo. Cancer Res. *71*, 7168–7175. https://doi.org/10.1158/0008-5472.CAN-11-0459.

6. Alexandrova, E.M., Yallowitz, A.R., Li, D., Xu, S., Schulz, R., Proia, D.A., Lozano, G., Dobbelstein, M., and Moll, U.M. (2015). Improving survival by exploiting tumour dependence on stabilized mutant p53 for treatment. Nature *523*, 352–356. https://doi.org/10.1038/nature14430.

7. Siegel, R.L., Miller, K.D., and Jemal, A. (2016). Cancer statistics, 2016. CA A Cancer J. Clin. *66*, 7–30. https://doi.org/10.3322/caac.21332.

8. Griffioen, G.H., Lagerwaard, F.J., Haasbeek, C.J., Smit, E.F., Slotman, B.J., and Senan, S. (2013). Treatment of multiple primary lung cancers using stereotactic radiotherapy, either with or without surgery. Radiother. Oncol. *107*, 403–408. https://doi.org/10.1016/j.radonc.2013.04.026.

9. Mogi, A., and Kuwano, H. (2011). TP53 mutations in nonsmall cell lung cancer. J. Biomed. Biotechnol. *2011*, 583929. https://doi.org/10.1155/2011/583929.

10. Miller, C.W., Simon, K., Aslo, A., Kok, K., Yokota, J., Buys, C.H., Terada, M., and Koeffler, H.P. (1992). p53 mutations in human lung tumors. Cancer Res. *52*, 1695–1698.

11. Reichel, M.B., Ohgaki, H., Petersen, I., and Kleihues, P. (1994). p53 mutations in primary human lung tumors and their metastases. Mol. Carcinog. *9*, 105–109. https://doi.org/10.1002/mc.2940090208.

12. Ahrendt, S.A., Hu, Y., Buta, M., McDermott, M.P., Benoit, N., Yang, S.C., Wu, L., and Sidransky, D. (2003). p53 mutations and survival in stage I non-small-cell lung cancer: results of a prospective study. J. Natl. Cancer Inst. *95*, 961–970. https://doi.org/10.1093/jnci/95.13.961.

13. Lim, E.H., Zhang, S.L., Li, J.L., Yap, W.S., Howe, T.C., Tan, B.P., Lee, Y.S., Wong, D., Khoo, K.L., Seto, K.Y., et al. (2009). Using whole genome amplification (WGA) of low-volume biopsies to assess the prognostic role of EGFR, KRAS, p53, and CMET mutations in advanced-stage non-small cell lung cancer (NSCLC). J. Thorac. Oncol. *4*, 12–21. https://doi.org/10.1097/JTO.0b013e3181913e28.

14. Ludovini, V., Pistola, L., Gregorc, V., Floriani, I., Rulli, E., Piattoni, S., Di Carlo, L., Semeraro, A., Darwish, S., Tofanetti, F.R., et al. (2008). Plasma DNA, microsatellite alterations, and p53 tumor mutations are associated with disease-free survival in radically resected non-small cell lung cancer patients: a study of the perugia multidisciplinary team for thoracic oncology. J. Thorac. Oncol. *3*, 365–373. https://doi.org/10.1097/JTO.0b013e318168c7d0.

15. Olivier, M., Hollstein, M., and Hainaut, P. (2010). TP53 mutations in human cancers: origins, consequences, and clinical use. Cold Spring Harbor Perspect. Biol. *2*, a001008. https://doi.org/10.1101/cshperspect.a001008.

16. Boettcher, S., Miller, P.G., Sharma, R., McConkey, M., Leventhal, M., Krivtsov, A.V., Giacomelli, A.O., Wong, W., Kim, J., Chao, S., et al. (2019). A dominant-negative effect drives selection of TP53 missense mutations in myeloid malignancies. Science (New York, N.Y.) *365*, 599–604. https://doi.org/10.1126/science.aax3649.

17. Yamamoto, S., and Iwakuma, T. (2018). Regulators of oncogenic mutant TP53 gain of function. Cancers *11*, 4. https://doi.org/10.3390/cancers11010004.

18. Giaccia, A.J., and Kastan, M.B. (1998). The complexity of p53 modulation: emerging patterns from divergent signals. Genes Dev. *12*, 2973–2983. https://doi.org/10.1101/gad.12.19.2973.

19. Xu, Z., Wu, W., Yan, H., Hu, Y., He, Q., and Luo, P. (2021). Regulation of p53 stability as a therapeutic strategy for cancer. Biochem. Pharmacol. *185*, 114407. https://doi.org/10.1016/j.bcp.2021.114407.

20. Li, M., Luo, J., Brooks, C.L., and Gu, W. (2002). Acetylation of p53 inhibits its ubiquitination by Mdm2. J. Biol. Chem. *277*, 50607–50611. https://doi.org/10.1074/jbc.C200578200.

21. Brooks, C.L., and Gu, W. (2011). The impact of acetylation and deacetylation on the p53 pathway. Protein Cell *2*, 456–462. https://doi.org/10.1007/s13238-011-1063-9.

22. Chen, H., Shan, J., Liu, J., Feng, Y., Ke, Y., Qi, W., Liu, W., and Zeng, X. (2020). RNF8 promotes efficient DSB repair by inhibiting the pro-apoptotic activity of p53 through regulating the function of Tip60. Cell Prolif. *53*, e12780. https://doi.org/10.1111/cpr.12780.

23. Laptenko, O., Shiff, I., Freed-Pastor, W., Zupnick, A., Mattia, M., Freulich, E., Shamir, I., Kadouri, N., Kahan, T., Manfredi, J., et al. (2015). The p53 C terminus controls site-specific DNA binding and promotes structural changes within the central DNA binding domain. Mol. Cell *57*, 1034–1046. https://doi.org/10.1016/j.molcel.2015.02.015.

24. Schneider, G. (2005). Enzymes in the biosynthesis of aromatic polyketide antibiotics. Curr. Opin. Struct. Biol. *15*, 629–636. https://doi.org/10.1016/j.sbi.2005.10.002.

25. Muller, P.A., and Vousden, K.H. (2013). p53 mutations in cancer. Nat. Cell Biol. *15*, 2–8. https://doi.org/10.1038/ncb2641.

26. Knowell, A.E., Patel, D., Morton, D.J., Sharma, P., Glymph, S., and Chaudhary, J. (2013). Id4 dependent acetylation restores mutant-p53 transcriptional activity. Mol. Cancer *12*, 161. https://doi.org/10.1186/1476-4598-12-161.

27. Perez, R.E., Knights, C.D., Sahu, G., Catania, J., Kolukula, V.K., Stoler, D., Graessmann, A., Ogryzko, V., Pishvaian, M., Albanese, C., and Avantaggiati, M.L. (2010). Restoration of DNA-binding and growth-suppressive activity of mutant forms of p53 via a PCAF-mediated acetylation pathway. J. Cell. Physiol. *225*, 394–405. https://doi.org/10.1002/jcp.22285.

28. Muller, P.A., and Vousden, K.H. (2014). Mutant p53 in cancer: new functions and therapeutic opportunities. Cancer Cell *25*, 304–317. https://doi.org/10.1016/j.ccr.2014.01.021.

29. Hafner, A., Bulyk, M.L., Jambhekar, A., and Lahav, G. (2019). The multiple mechanisms that regulate p53 activity and cell fate. Nat. Rev. Mol. Cell Biol. *20*, 199–210. https://doi.org/10.1038/s41580-019-0110-x.

30. Reed, S.M., and Quelle, D.E. (2014). p53 acetylation: regulation and consequences. Cancers *7*, 30–69. https://doi.org/10.3390/cancers7010030.

31. Krummel, K.A., Lee, C.J., Toledo, F., and Wahl, G.M. (2005). The C-terminal lysines fine-tune P53 stress responses in a mouse model but are not required for stability control or transactivation. Proc. Natl. Acad. Sci. USA *102*, 10188–10193. https://doi.org/10.1073/pnas.0503068102.

32. Chen, H., Zhang, W., Cheng, X., Guo, L., Xie, S., Ma, Y., Guo, N., and Shi, M. (2017). beta2-AR activation induces chemoresistance by modulating p53 acetylation through upregulating Sirt1 in cervical cancer cells. Cancer Sci. *108*, 1310–1317. https://doi.org/10.1111/cas.13275.

33. Park, J.H., Yang, S.W., Park, J.M., Ka, S.H., Kim, J.H., Kong, Y.Y., Jeon, Y.J., Seol, J.H., and Chung, C.H. (2016). Positive feedback regulation of p53 transactivity by DNA damage-induced ISG15 modification. Nat. Commun. *7*, 12513. https://doi.org/10.1038/ncomms12513.

34. Soragni, A., Janzen, D.M., Johnson, L.M., Lindgren, A.G., Thai-Quynh Nguyen, A., Tiourin, E., Soriaga, A.B., Lu, J., Jiang, L., Faull, K.F., et al. (2016). A designed inhibitor of p53 aggregation rescues p53 tumor suppression in ovarian carcinomas. Cancer Cell *29*, 90–103. https://doi.org/10.1016/j.ccell.2015.12.002.

35. Palanikumar, L., Karpauskaite, L., Al-Sayegh, M., Chehade, I., Alam, M., Hassan, S., Maity, D., Ali, L., Kalmouni, M., Hunashal, Y., et al. (2021). Protein mimetic amyloid inhibitor potently abrogates cancer-associated mutant p53 aggregation and restores tumor suppressor function. Nat. Commun. *12*, 3962. https://doi.org/10.1038/s41467-021-23985-1.

36. Kanapathipillai, M. (2018). Treating p53 mutant aggregation-associated cancer. Cancers *10*, E154. https://doi.org/10.3390/cancers10060154.

37. Kong, L.R., Ong, R.W., Tan, T.Z., Mohamed Salleh, N.A., Thangavelu, M., Chan, J.Y., Koh, L.Y., Periyasamy, G., Lau, J.A., Le, T.B., et al. (2020). Targeting codon 158 p53-mutant cancers via the induction of p53 acetylation. Nat. Commun. *11*, 2086. https://doi.org/10.1038/s41467-020-15608-y.

38. Hanel, W., Marchenko, N., Xu, S., Yu, S.X., Weng, W., and Moll, U. (2013). Two hot spot mutant p53 mouse models display differential gain of function in tumorigenesis. Cell Death Differ. *20*, 898–909. https://doi.org/10.1038/cdd.2013.17.

39. He, C., Li, L., Guan, X., Xiong, L., and Miao, X. (2017). Mutant p53 gain of function and chemoresistance: the role of mutant p53 in response to clinical chemotherapy. Chemotherapy *62*, 43–53. https://doi.org/10.1159/000446361.

40. Nguyen, T.A., Menendez, D., Resnick, M.A., and Anderson, C.W. (2014). Mutant TP53 posttranslational modifications: challenges and opportunities. Hum. Mutat. *35*, 738–755. https://doi.org/10.1002/humu.22506.

41. La Fleur, L., Falk-Sörqvist, E., Smeds, P., Berglund, A., Sundström, M., Mattsson, J.S., Brandén, E., Koyi, H., Isaksson, J., Brunnström, H., et al. (2019). Mutation patterns in a population-based non-small cell lung cancer cohort and prognostic impact of concomitant mutations in KRAS and TP53 or STK11. Lung Cancer *130*, 50–58. https://doi.org/10.1016/j.lungcan.2019.01.003.

42. Saleh, M.M., Scheffler, M., Merkelbach-Bruse, S., Scheel, A.H., Ulmer, B., Wolf, J., and Buettner, R. (2022). Comprehensive analysis of TP53 and KEAP1 mutations and their impact on survival in localized- and advanced-stage NSCLC. J. Thorac. Oncol. *17*, 76–88. https://doi.org/10.1016/j.jtho.2021.08.764.

43. Kennedy, M.C., and Lowe, S.W. (2022). Mutant p53: it's not all one and the same. Cell Death Differ. *29*, 983–987. https://doi.org/10.1038/s41418-022-00989-y.

44. Freed-Pastor, W.A., and Prives, C. (2012). Mutant p53: one name, many proteins. Genes Dev. *26*, 1268–1286. https://doi.org/10.1101/gad.190678.112.

45. Yang, L., Song, T., Cheng, Q., Chen, L., and Chen, J. (2019). Mutant p53 sequestration of the MDM2 acidic domain inhibits E3 ligase activity. Mol. Cell Biol. *39*. e00375–18. https://doi.org/10.1128/MCB.00375-18.

46. Campbell, J.D., Alexandrov, A., Kim, J., Wala, J., Berger, A.H., Pedamallu, C.S., Shukla, S.A., Guo, G., Brooks, A.N., Murray, B.A., et al. (2016). Distinct patterns of somatic genome alterations in lung adenocarcinomas and squamous cell carcinomas. Nat. Genet. *48*, 607–616. https://doi.org/10.1038/ng.3564.

47. Fan, Z., Zhang, Q., Feng, L., Wang, L., Zhou, X., Han, J., Li, D., Liu, J., Zhang, X., Zuo, J., et al. (2022). Genomic landscape and prognosis of patients with TP53-mutated non-small cell lung cancer. Ann. Transl. Med. *10*, 188. https://doi.org/10.21037/atm-22-412.

48. Zhang, N., Wu, J., Yu, J., Zhu, H., Yang, M., and Li, R. (2020). Integrating imaging, histologic, and genetic features to predict tumor mutation burden of non-small-cell lung cancer. Clin. Lung Cancer *21*, e151–e163. https://doi.org/10.1016/j.cllc.2019.10.016.

49. Poeta, M.L., Manola, J., Goldwasser, M.A., Forastiere, A., Benoit, N., Califano, J.A., Ridge, J.A., Goodwin, J., Kenady, D., Saunders, J., et al. (2007). TP53 mutations and survival in squamous-cell carcinoma of the head and neck. N. Engl. J. Med. *357*, 2552–2561. https://doi.org/10.1056/NEJMoa073770.

50. Asher, G., Lotem, J., Tsvetkov, P., Reiss, V., Sachs, L., and Shaul, Y. (2003). P53 hot-spot mutants are resistant to ubiquitin-independent degradation by increased binding to NAD(P)H:quinone oxidoreductase 1. Proc. Natl. Acad. Sci. USA *100*, 15065–15070. https://doi.org/10.1073/pnas.2436329100.

51. Li, D., Marchenko, N.D., and Moll, U.M. (2011). SAHA shows preferential cytotoxicity in mutant p53 cancer cells by destabilizing mutant p53 through inhibition of the HDAC6-Hsp90 chaperone axis. Cell Death Differ. *18*, 1904–1913. https://doi.org/10.1038/cdd.2011.71.

52. Hiraki, M., Hwang, S.Y., Cao, S., Ramadhar, T.R., Byun, S., Yoon, K.W., Lee, J.H., Chu, K., Gurkar, A.U., Kolev, V., et al. (2015). Small-molecule reactivation of mutant p53 to wild-type-like p53 through the p53-hsp40 regulatory Axis. Chem. Biol. *22*, 1206–1216. https://doi.org/10.1016/j.chembiol.2015.07.016.

53. Birsen, R., Larrue, C., Decroocq, J., Johnson, N., Guiraud, N., Gotanegre, M., Cantero-Aguilar, L., Grignano, E., Huynh, T., Fontenay, M., et al. (2022). APR-246 induces early cell death by ferroptosis in acute myeloid leukemia. Haematologica *107*, 403–416. https://doi.org/10.3324/haematol.2020.259531.

54. Muller, P., Hrstka, R., Coomber, D., Lane, D.P., and Vojtesek, B. (2008). Chaperone-dependent stabilization and degradation of p53 mutants. Oncogene *27*, 3371–3383. https://doi.org/10.1038/sj.onc.1211010.

55. Lukashchuk, N., and Vousden, K.H. (2007). Ubiquitination and degradation of mutant p53. Mol. Cell Biol. *27*, 8284–8295. https://doi.org/10.1128/MCB.00050-07.

56. Jiao, J., Zhang, R., Li, Z., Yin, Y., Fang, X., Ding, X., Cai, Y., Yang, S., Mu, H., Zong, D., et al. (2018). Nuclear Smad6 promotes gliomagenesis by negatively regulating PIAS3-mediated STAT3 inhibition. Nat. Commun. *9*, 2504. https://doi.org/10.1038/s41467-018-04936-9.

57. Wang, J., Huang, Z., Ji, L., Chen, C., Wan, Q., Xin, Y., Pu, Z., Li, K., Jiao, J., Yin, Y., et al. (2022). SHF acts as a novel tumor suppressor in glioblastoma multiforme by disrupting STAT3 dimerization. Adv. Sci. *9*, e2200169. https://doi.org/10.1002/advs.202200169.

58. Soussi, T. (2007). Handbook of P53 Mutation in Cell Lines, 07 Edition. Version 1.

59. Yin, Y., Zhang, X., Li, Z., Deng, L., Jiao, G., Zhang, B., Xie, P., Mu, H., Qiao, W., and Zou, J. (2013). Glucocorticoid receptor beta regulates injury-mediated astrocyte activation and contributes to glioma pathogenesis via modulation of beta-catenin/TCF transcriptional activity. Neurobiol. Dis. *59*, 165–176. https://doi.org/10.1016/j.nbd.2013.07.013.

60. Wang, Q., Lu, P.H., Shi, Z.F., Xu, Y.J., Xiang, J., Wang, Y.X., Deng, L.X., Xie, P., Yin, Y., Zhang, B., et al. (2015). Glucocorticoid receptor beta acts as a Co-activator of T-cell factor 4 and enhances glioma cell proliferation. Mol. Neurobiol. *52*, 1106–1118. https://doi.org/10.1007/s12035-014-8900-9.

61. Asp, M., Giacomello, S., Larsson, L., Wu, C., Fürth, D., Qian, X., Wärdell, E., Custodio, J., Reimegård, J., Salmén, F., et al. (2019). A spatiotemporal organ-wide gene expression and cell Atlas of the developing human heart. Cell *179*, 1647–1660.e19. https://doi.org/10.1016/j.cell.2019.11.025.

STAR★METHODS

KEY RESOURCES TABLE

REAGENT or RESOURCE	SOURCE	IDENTIFIER
Antibodies		
Mouse anti-GAPDH	Proteintech	Cat# 60004-1-Ig; RRID: AB_2107436
Mouse HA-tag	Abmart	Cat# M20003; RRID: AB_2864345
Rabbit Ubiquitin	ABCAM	Cat# ab7780; RRID: AB_306069
Mouse anti-p53	Sigma	Cat# P5813; RRID: AB_261106
Rabbit Ac-Lysine	ABCAM	Cat# ab21623; RRID: AB_446436
Rabbit anti-p53 (acetyl K382)	ABCAM	Cat# ab75754; RRID: AB_1310532
Rabbit anti-p53 (acetyl K373)	ABCAM	Cat# ab62376; RRID: AB_944589
Peroxidase AffiniPure Goat Anti-Mouse IgG, light chain specific	Jacson ImmunoReseatch	Cat# 115-035-174; RRID: AB_2338512
Peroxidase IgG Fraction Monoclonal Mouse Anti-Rabbit IgG, light chain specific	Jacson ImmunoReseatch	Cat# 211-032-171; RRID: AB_2339149
Goat anti-mouse IgG (H + L) HRP conjugate	Proteintech	Cat# SA00001-1; RRID: AB_2722565
Goat anti-rabbit IgG (H + L) HRP conjugate	Proteintech	Cat# SA00001-2; RRID: AB_2722564
Bacterial and virus strains		
GV348-TP53-HA	Genechem	N/A
GV348-R175H-HA	Genechem	N/A
GV348-TP53-3KQ-HA	Genechem	N/A
GV348-R175H-3KQ-HA	Genechem	N/A
GV348-TP53-6KR-HA	Genechem	N/A
GV348-R175H-6KR-HA	Genechem	N/A
Chemicals, peptides, and recombinant proteins		
ReAcp53	MedChemExpress	Cat# HY-P0121
Cycloheximide	Selleck	Cat# S7418
Etoposide	Selleck	Cat# S1225
Doxorubicin	Selleck	Cat# E2516
Critical commercial assays		
SimpleChIP® Enzymatic Chromatin IP Kit	Cell Signaling	Cat# 91820
EdU incorporation assay Kit	KeyGen Biotech	Cat# KGA337-500
Apoptosis Detection Kit	KeyGen Biotech	Cat# KGA105
HiFiScript cDNA Synthesis Kit	Cwbio	Cat# CW2569M
Oligonucleotides		
Primers for RT-qPCR assay	Sangon	Table S2
Primers for ChIP-qPCR assay	Sangon	Table S3
Deposited data		
NSCLC samples data	This paper	https://www.cbioportal.org
Transcriptome sequencing and data	This paper	http://www.scidb.cn
Software and algorithms		
GraphPad Prism	GraphPad	https://www.graphpad.com
FlowJo	FlowJo	https://www.flowjo.com
GSEA	Broad Institute	http://software.broadinstitute.org/gsea/index.jsp
R	R-Project	https://www.rproject.org

RESOURCE AVAILABILITY

Lead contact

Further information and requests for resources and reagents should be directed to and will be fulfilled by the Lead Contact, Jian Zou (zoujan@njmu.edu.cn).

Materials availability

All unique reagents generated in this study are available from the lead contact with a completed Materials Transfer Agreement.

Data and code availability

- Data from in-house cohorts are available from the corresponding author on reasonable request. Data from publicly archive datasets are available from cBioPortal, CPTAC database, as publications cited in the manuscript. These accession numbers for the datasets are also listed in the method details.
- Code: This paper does not report original code.
- All other requests: Any additional information required to reanalyze the data reported in this paper is available from the lead contact upon request.

EXPERIMENTAL MODEL AND SUBJECT DETAILS

Cell lines

The human NSCLC cell lines H1299, A549, H446, PC-9, and H520 were obtained from the Cell Bank of Type Culture Collection of the Chinese Academy of Sciences. All cells were cultured in DMEM with 10% fetal bovine serum (BI, Kibbutz, Israel). These cells were characterized by Genewiz, Inc. (China) using short tandem repeat markers and were confirmed to be mycoplasma-free (last tested in 2021).

Clinical sample and immunohistochemical staining

The LUAD tissue microarray was used to perform immunohistochemical (IHC) staining of p53 and acetylated p53 (Ac-p53) expression. It contained 82 LUAD samples and their adjacent non-cancerous tissue (NCT), as well as another 16 LUAD samples. The tissue microarray and clinical information (Table S1) was obtained from Shanghai Outdo Biotech (HLugA180Su07). The IHC procedure was performed as described in our previous studies.[56,57] The slides were incubated with primary antibodies. Cell nuclei were counterstained lightly with crystal violet. The specificity of IHC was confirmed by normal mouse or rabbit IgG. The expression of target proteins was semi-quantitatively scored according to an established immunoreactivity scoring (IRS) system.[56] Two blinded pathologists independently scored the slides, and the mean IRS score was considered as the final (Table S1).

Tumor xenografts in nude mice

Four-week-old male nude mice were obtained from the Changzhou Cavens Experimental Animal Co., Ltd (Jiangsu, China) and held under specific pathogen-free conditions. 5 x 10^6 H1299 cells expressing Mock, R175H or R175H3KQ in 100 μL of DMEM: Matrigel (8:1, v/v; BD Biosciences, Franklin Lakes, NJ) were injected s.c. into the right flank of each mouse. After forming a mass visible tumor, tumor growth was subsequently monitored by measuring tumor diameter at the indicated times by blinded researchers. At the final day, mice were euthanized and tumors were collected, weighed, and measured. For determine the tumor inhibition of ReAcp53, mice were implanted with H1299-R175H cells in the same way. When the derived tumors developed about 200 mm^3 and were segmented into pieces of 1 mm^3. Mice were randomly grouped and implanted with one tumor segmentation and received intraperitoneal injections of DMSO or ReAcp53 (15 mg/kg) every day for 14 days. Tumor volume was monitored as indicated from the first treatment. Tumors were collected on the 15th day post-first treatment and tumor weight was measured. All animal care and handling procedures were performed in accordance with the National Institutes of Health's Guide for the Care and Use of Laboratory Animals and were approved by the Institutional Review Board of Nanjing Medical University. No mice were excluded from scoring.

METHOD DETAILS

Online cancer database acquisition and analysis

Data visualization and exploration of *TP53* mutation information in NSCLC samples was implemented through cBioPortal for Cancer Genomics (cBioPortal: https://www.cbioportal.org/). A total of 17 previous studies (Lung adenocarcinoma: Broad, Cell 2012, MSKCC, Science 2015, OncoSG, Nat Genet 2020, TCGA, Firehose Legacy, TCGA, Nature 2014, TCGA, Pan Cancer Atlas, TSP, Nature 2008; Lung squamous cell carcinoma: TCGA, Firehose Legacy, TCGA, Nature 2012, TCGA, Pan Cancer Atlas; Non-small cell lung cancer: MSKCC, Cancer Discov 2017, MSK, Cancer Cell 2018, MSK, Science 2015, MSKCC, J Clin Oncol 2018, TRACERx, NEJM & Nature 2017, University of Turin, Lung Cancer 2017 and Pan-lung Cancer: TCGA, Nat Genet 2016) including 6122 samples from 5718 patients were accepted for follow-up analyses and image presentation. Pre-processing RNA expression data, details of *TP53* mutation status, putative copy number variation (CNV) status, and corresponding clinical information of LUAD and lung squamous cell carcinoma (LUSC) were obtained from the download module of cBioPortal (TCGA, Pan Cancer Atlas). Count reads were normalized with log2 transformation after adding a 0.5 pseudocount to avoid logical error. The protein data was acquired from The Clinical Proteomic Tumor Analysis Consortium (CPTAC). Only those containing single or multiple p53 missense mutation sites were defined as missense mutations, while those with other mutation forms were excluded from the category of missense mutations. Cell line data (DepMap Public 22Q2) was derived from CCLE browser (CCLE: https://sites.broadinstitute.org/ccle/). By integrating Cellosaurus (Cellosaurus: https://web.expasy.org/cellosaurus/) and other reports,[58] CORL105, NCIH1944, NCIH1666, SW1573, A549, A427, NCIH1563 and DV90 were determined to be NSCLC cell lines with wild type p53 expression.

Gene enrichment assay

Gene enrichment assay was performed by Gene Set Variation Analysis (GSVA) and Gene Set Enrichment Analysis (GSEA) according the gene sets of 'h.all.v7.5.1.symbols' in the MSigDB database. GSVA was analyzed by "GSVA" R package (Version 1.38.2) and presented by "ggplot2" R package (Version 3.3.5). GSEA was performed using Java desktop software (Version 4.1.0). The significance threshold was set at | t value |>2, | Normalized Enrichment Score | >1, and nominal P-value <0.05.

Vector construction and transduction

Full-length cDNA encoding human *TP53* (NM_000546.5) was amplified by PCR and verified by DNA sequencing. p53-HA lentivirus was constructed by inserting cDNA sequence into lentivirus vector GV348 (Genechem, Shanghai, China) with a hemagglutinin (HA)-tag. p53-R175H mutant (R175H-HA) lentivirus was constructed based on the wild-type p53 lentivirus. As shown in Figure S3A, the CTD constitutive acetylation mutants (3KQ) were constructed based on p53 and R175H lentivirus with amino acid mutations to glutamine (Q) at K373, K381 and K382, and the CTD non-acetylation mutants (6KR) were constructed based on p53 and R175H lentivirus with amino acid mutations to arginine (R) at K370, K372, K373, K381, K382, K386.

Western blot assay

The expression of target proteins was measured by standard Western blot as previously described.[59] Cells were lysed by RIPA lysis buffer (Cell Signal Technology, Beverly, MA), and protein concentration was measured by bicinchoninic acid (BCA) assay (CWBIO, China). For p53 acetylation analysis, cells were treated with or without Doxorubicin (Dox, Selleck, Houston, TX) at concentrations of 1 μM for 2 h. For protein stability analysis, cells were treated with cycloheximide (CHX, 20 μg/mL; Sigma-Aldrich, St Louis, MO) for the indicated times to block protein synthesis. Cell lysates were performed by standard Western blot assay with the indicated antibodies to detect the target proteins degradation. For protein solution assay, cells were treated with ReAcp53 (MedChemExpress, New Jersey, NJ) at concentrations of 5 μM for 16–20 h.[34] Cell pellets were washed twice with PBS and lysed in RIPA lysis buffer supplemented with phosphatase inhibitors for 30 min on ice. Soluble supernatant and insoluble precipitation of lysates were obtained by centrifugation (12, 000 rpm) at 4°C. All lysates were diluted in loading buffer and denatured by heating at 100°C. The prepared samples were analyzed by Western blot. Antibodies used to determine the indicated proteins are shown in key resources table.

Immunoprecipitation (IP) assays

IP experiments were performed to analyze protein ubiquitination. Briefly, cells were lysed by RIPA Lysis Buffer and the whole-cell lysates were precipitated using Protein A/G magnetic beads (Bimake, TX, USA) with hemagglutinin (HA) tag antibody. Precipitated products were analyzed by Western blot using Ubiquitin (Ub) or HA antibody subsequently. The indicated protein expressed in total lysates were detected by Western blot.

p53 transcriptional reporter assay

The reporter construct, pGL4.38[luc2P/p53 RE/Hygro] (p53 RE-pGL4.38, Promega, Madison, WI) was used to evaluate p53 transcriptional activity. H1299 cells with indicated p53 constructs were transiently transfected with the vector. pRL-TK Renilla luciferase plasmid (Promega) acted as a control. Thirty six hours after transfection, p53 transcriptional activity was measured by a luciferase reporter system (Promega, Madison, WI) according to our previously study.[56]

Transcriptome sequencing and data analysis

Transcriptome sequencing service was provided by YiKe Population Health Research Institute (China). Briefly, total RNA of indicated cells cultured for 48 h was exacted using Trizol reagent (Thermo Fisher, MA), qualified by NanoPhotometer (IMPLEN, CA) and quantified by Qubit 3.0 Flurometer C (Thermo Fisher). The captured mRNA with polyA tail was transcribed to double strand cDNA and sequenced on a HiSeq3000 system (Illumina, San Diego, CA) after library construction. Raw reads were acquired by CASAVA v1.8 and stored in FASTQ format. Human reference genome (GRCh37) was used to align the aforementioned reads. Statistical results in term of "Read counts" were output through Htseq v0.7.2 and corresponding "FPKM (Reads Per Kilo bases per Million reads)" were also calculated. GSEA was performed on the basis of sequencing data between the indicated groups. H1299 cells containing various constructs with 3 duplicates for a total of 15 samples underwent sequencing and data analysis.

Cell growth and colony formation assay

Cell growth was assayed using the Cell Counting Kit-8 Kit (Biotool, Houston, TX). Each experiment was performed with six independent biological samples with six technical replicates each time. For the colony formation assay, 200 cells were seeded into each well of a six-well plate with soft agar (Agarose; Sigma--Aldrich) and maintained in a medium containing 10% FBS for 14 days. At the final culture day, the colonies were fixed with methanol and stained with 0.1% crystal violet. The clones containing 50 cells were counted using an inverted microscope. Colony formation assay was performed with three biological samples, independently (three technical replicates each time).

Cell cycle assay

Cells were cultured for 24 h and synchronized by serum deprivation for 24 h. Next, cells were re-cultured in normal medium for another 24 h, harvested, and fixed with 70% ethanol at −20°C. The derived cells were suspended in PBS containing 100 ng/mL of RNaseA (Boehringer Mannheim, Indianapolis, IN) and incubated with 50 μg/mL of propidium iodide (PI, Sigma-Aldrich) for 1 h at RT protected from light exposure. Cell cycle fractions were measured by FACS Canto II (BD, Mountain View, CA), and the percentages of cells in G1, S and G2 phases were calculated using ModFit LT software (RRID:SCR_016106, BD).

EdU incorporation assay

EdU incorporation was used to detect DNA replication as described previously.[60] Briefly, cells were cultured on coverslips coated with polylysine (20 μg/mL; Sigma-Aldrich) for 36 h in 24-well plates and subsequently incubated with EdU (Keygen Biotech, China) for 12 h, followed by fixation. The staining procedure was performed according to the manufacturer's instructions (Keygen Biotech, China). The coverslips were mounted with Gelmount containing Hoechst 33342 (Sigma-Aldrich). The quantitative results were expressed as the percentage of EdU positive cells out of the total number of cells (as labeled with Hoechst).

3D-spheroid formation and growth measurement

3D-Spheroid formation and growth assay was performed as described previously.[56,57] Briefly, the detached cells were resuspended in GBO medium with a minor modification (without insulin) according to a previously published report.[61] Cells were seeded in the non-adherent 96-well plate (Corning, NY) at 400

cells/well. Half of the medium was changed every 2 days. The spheroid formation and growth was monitored by a microscope with a real-time camera (EVOS FL Auto Imaging System, Life Technologies, Carlsbad, CA, USA). Photographs of tumor spheres were taken at the indicated time points and the area of the spheroids was measured to reflect the growth status over time.

Cell apoptosis analysis

Cell apoptosis was assayed by Flow cytometry according to the manufacturer's instruction of the Apoptosis Detection Kit (KeyGen Biotech, China). Briefly, cells were cultured for 36 h and incubated with Dox (0.5 μM) and Etoposide (Eto, 10μM; Selleck, Houston, TX) for 24 h before harvest. After incubation with Annexin V-FITC/propidium iodide (PI), cells were immediately analyzed by FACScan flow cytometry (Becton–Dickinson, Mountain View, CA, USA).

Reverse-transcription quantitative PCR (RT-qPCR)

RT-PCR was performed to measure the targeted genes expression. Cells were treated with Dox (0.5 μM) for 24 h and total RNA was extracted using TRIzol reagent (Invitrogen) according to the manufacturer's instructions. cDNA was synthesized with the HiFiScript cDNA Synthesis Kit (Cwbio, Beijing, China), and PCR analyses were conducted using UltraSYBR Mixture (Cwbio) on a Lightcycler 480 II instrument (Roche Applied Science). GAPDH severed as an internal control. The specific oligonucleotide primer pairs are listed in Table S2.

ChIP and ChIP-qPCR assays

The ChIP and ChIP-qPCR assays were performed to determine p53-DNA binding ability. ChIP was conducted according to the manufacturer's instructions for the SimpleChIP Enzymatic Chromatin IP Kit (Cell Signaling, Inc., Danvers MA). In brief, $2x10^7$ cells and 7.5 μg anti-p53 antibody were used for each ChIP. Mouse IgG and rabbit anti-Histone H3 antibody severed as negative control and positive control, respectively. After reversal of cross-links and DNA purification, samples were used for qPCR with specific primers targeting gene promoters (Table S3). ChIP efficiency was expressed according to our previously established method.[57]

QUANTIFICATION AND STATISTICAL ANALYSIS

Data were expressed as mean ± SD. Differences were determined by a statistical significance of $p < 0.05$, $^*p < 0.05$, $^{**}p < 0.01$, $^{***}p < 0.001$. For the analyses of public bulk data, the variables were examined for normal distribution by the Shapiro-Wilk normality test. If the samples obeyed normal distribution and had equal variances, unpaired t tests were selected for analysis. Otherwise, Wilcoxon rank-sum test was applied. Survival analyses were performed using the Kaplan-Meier method with log rank test. The optimal cut-off values were determined by X-tile. The difference between two independent samples and multiple experimental groups was determined by Student t test or one-way analysis of variance (ANOVA) followed by a Newman Keuls' multiple comparison test respectively. All statistical analyses and data graphing were performed by FlowJo V10, Graphpad prism 8.0 or R.

ADDITIONAL RESOURCES

No additional resources are available for this article.